Restricted-space *ab initio* models for double ionization by strong laser pulses

Dmitry K. Efimov,[1,*] Artur Maksymov,[1] Jakub S. Prauzner-Bechcicki,[1] Jan H. Thiede,[2] Bruno Eckhardt,[2] Alexis Chacón,[3,4] Maciej Lewenstein,[4,5] and Jakub Zakrzewski[1,6]

[1]*Instytut Fizyki Imienia Mariana Smoluchowskiego, Uniwersytet Jagielloński, Łojasiewicza 11, 30-348 Kraków, Poland*

[2]*Philipps-University Marburg, Biegenstraße 10, 35037 Marburg, Germany*

[3]*Center for Nonlinear Studies, Theoretical Division, Los Alamos National Laboratory, Los Alamos, New Mexico 87545, USA*

[4]*ICFO - Institut de Ciencies Fotoniques, The Barcelona Institute of Science and Technology, Av. Carl Friedrich Gauss 3, 08860 Castelldefels (Barcelona), Spain*

[5]*ICREA, Pg. Lluís Companys 23, 08010 Barcelona, Spain*

[6]*Mark Kac Complex Systems Research Center, Jagiellonian University, Łojasiewicza 11, 30-348 Kraków, Poland*

(Received 29 March 2018; published 11 July 2018)

A double-electron-ionization process occurs when an intense laser pulse interacts with atoms or molecules. Exact *ab initio* numerical simulation of such a situation is extremely computer resource demanding, thus often one is forced to apply reduced dimensionality models to get insight into the physics of the process. The performance of several algorithms for simulating double electron ionization by strong femtosecond laser pulses is studied. The obtained ionization yields and the momentum distributions of the released electrons are compared and the effects of the model dimensionality on the ionization dynamics are discussed.

DOI: 10.1103/PhysRevA.98.013405

I. INTRODUCTION

A number of noteworthy phenomena occur during interactions of atoms and molecules with short strong laser pulses, for example, high-order harmonic generation (HHG) and nonsequential double ionization (NSDI). As experiments in strong-field physics become more refined, there is an increasing demand for performing *ab initio* simulations that could provide insight into observed phenomena. Several methods have been developed in that respect over the past 20 years. However, quite surprisingly, it is rather difficult to find a comparison between various proposed approaches. This is the primary aim of the present contribution. We will concentrate on ionization of the He atom as the simplest two-electron system.

Ideally, the experimental data are to be simulated with full-dimensional theoretical models [1,2]. However, a full-scale simulation requires huge computational resources. Practically, for low laser frequencies, it is doable only for systems within a single-active-electron approximation [3]. Thus, already two-electron correlation effects are almost beyond the scope of possibilities of the full-dimensional quantum treatment; the only calculations performed in such a way in [1,4,5] are very hard to implement technically. These calculations, treating double-electron effects, were performed exclusively for laser pulses with a carrier frequency in the UV spectral range, while most experiments deal with infrared and midinfrared ranges, which makes applications of the full grid-based methods limited. Realistically, one is limited to design and use unsophisticated models with a reduced number of dimensions. The hardest part is to judiciously choose a coordinate system that, on one hand, captures "all the important physics" of the treated phenomena and, on the other, is reasonably tractable with available hardware and software resources. Finally, one has to admit that these low-dimensional models inevitably lack the precision and the predictive power of full-scale simulations.

Nevertheless, most of the effects and tendencies observed in double ionization are surprisingly well described, at least qualitatively, by models with reduced dimensionality [6]. This concerns, in particular, NSDI, in which two electrons, after an initial excitation of one of them, share the excitation energy and ionize together. Among the most prominent features, the knee structure in the double-ionization yields, found in numerous experiments [7,8], was successfully simulated within the quantum-mechanical two-dimensional (2D) models [9–12] as well as with its classical analogs [13,14]. The fingerlike structure of released electron momenta, obtained experimentally in [15–18], was reproduced with quantum [11,19] and classical [20] simulations. At the same time, other results, such as the theoretical prediction of the second plateau in high-harmonic-generation spectra [21], have not been verified experimentally yet (to our knowledge) mainly because of the presently inaccessibly high precision needed for their investigation. All the reduced dimensionality models employ a linearly polarized field, as a system affected by an elliptically polarized field necessarily needs the full dimensionality studies.

The first (and the simplest) restricted dimensionally two-electron model implemented is the so-called aligned electrons, or Rochester model [22]. With the nuclear motion not taken into an account, the $3 + 3 = 6$ dimensions of the problem are reduced to 2, each one corresponding to the z coordinate of an electron, where z is collinear with the electric-field direction. This model allowed one to observe the well pronounced knee structure [9], as well as the momentum distribution [23]. The most striking disadvantage of the method is due to the distortions in the double-ionization data: Electrons are not allowed to escape with similar momenta because of the

*dmitry.efimov@uj.edu.pl

dominant effect of the Coulomb repulsion in the restricted geometry.

This problem of the aligned-electron model has been eliminated in the Eckhardt-Sacha model by spatially separating the two axes [24]. Their direction is determined by the lines drawn by saddles of the field when its amplitude is varied. Those lines are at the angle of $\pm\pi/6$ with respect to the z axis. While necessarily the reduced dimensionality has obvious drawbacks (e.g., considering the motion along the saddle lines only neglecting possible optimal paths across the saddles in full space), this model overcomes the obvious drawbacks of the aligned electrons model. As a result, more reliable data for both ionization yield and momentum distribution were obtained for the Eckhardt-Sacha (ES) model by Prauzner-Bechcicki and co-workers (the ES approach) [11,12,25].

Another approach was proposed by Ruiz *et al.* [26], by making reasonable assumptions about the motion of electrons in the laser field. In the center-of-mass (c.m.) representation and with linear polarization for the laser light one may assume that the c.m. moves along the polarization axis. The resulting model yielded a striking success in reproducing the experimentally obtained parallel momentum distribution (momenta parallel to the z axis) [19].

All these geometries, the aligned-electron, the ES, the c.m., or even the full dimensionality models, can be implemented in classical simulations. The key idea is to mimic the evolution of electronic systems in terms of classical trajectories that are sampled from an initial phase-space distribution and are governed by classical Hamiltonian dynamics [27]. Two groups of methods can be be distinguished: one with initial distributions calculated classically [27–32] and one accounting for below-barrier tunneling for initial distribution calculation [33]. The first group is the most instructive one for a comparison of the data with corresponding quantum-mechanical computations. Considerable progress was made with these models in the study of ionization yields [34,35] and momentum distributions [13]. On the other hand, getting HHG spectra with classical means only seems impossible (see, however, [36]). In particular, the extent of the plateau depends on the quantum ionization energy.

Generally, one can take some trusted analytical expressions as a reference. An important milestone in theoretical studies of atomic ionization was the creation of the Ammosov-Delone-Krainov (ADK) formula [37] that provides an extremely simple expression for the single-tunneling-ionization probability. It proved its reliability in comparison with numerous experimental data [7,8,38,39]. So far, it can be used for comparison of the single-ionization yield in different models. It is important to note, however, that the ADK rates are usually multiplied by an artificial constant factor to fit measured curves, thus one should be careful when treating absolute magnitudes.

Here we aim to compare the performance of the different computational models in determining the following experimental observables: yield of single ionization and of double ionization and momentum distribution of the released electrons. We will focus our attention on the ES and c.m. models, as they seem to be the most advanced. The aim is to see how well they are able to reproduce the experimental features qualitatively: We cannot expect that reduced-dimensionality models of this or any other type can be in quantitative agreement with experiments or truly three-dimensional simulations because of the vastly different phase-space volumes and ratios. Nevertheless, as we will have to rely on low-dimensional models for some time to come, it will be interesting to see how they compare.

In Sec. II we describe the algorithms used. In Sec. III we present a comparison of ionization yields and explain the observed differences. Section IV deals with a comparison of electronic momenta. A summary and conclusions are given in Sec.V. We stress that our aim is not to find the model yielding the "most accurate," i.e., in closest agreement with the experiment, prediction. This is not possible for reduced-dimensionality models. The models may serve to qualitatively describe experimental observations only. Still, it is interesting to compare even the qualitative predictions different models yield. We are not aware of any such an earlier comparison. Throughout the text we use atomic units, unless stated otherwise.

II. DESCRIPTION OF THE ALGORITHM

A. General remarks

The quantum algorithms for both models are based on the operator splitting method. In short, once one has a Hamiltonian for the problem under consideration in the form of $H = H_1 + H_2$, the solution of the corresponding time-dependent Schrödinger equation (TDSE) for a wave function $\Psi(t)$ for a small time interval Δt can be expressed according to the Suzuki-Trotter decomposition as

$$\Psi(t_0+\Delta t) \sim \exp\left(-i H_1 \frac{\Delta t}{2}\right) \exp(-i H_2 \Delta t) \times \exp\left(-i H_1 \frac{\Delta t}{2}\right) \Psi(t_0). \quad (1)$$

The wave function $\Psi(t_0+\Delta t)$ is obtained by sequentially propagating the initial wave function $\Psi(t_0)$ (from right to left) with the Hamiltonian H_1 for a time $\Delta t/2$, then with H_2 for a time Δt, and then again with H_1 for a time $\Delta t/2$. For a larger number of terms in the Hamiltonian, one can expand the formula in a straightforward manner. For instance, if $H_2 = H_3 + H_4$ then one can write

$$\exp(-i H_2 \Delta t) \sim \exp\left(-i H_3 \frac{\Delta t}{2}\right) \times \exp(-i H_4 \Delta t) \exp\left(-i H_3 \frac{\Delta t}{2}\right) \quad (2)$$

and propagate sequentially as in the previous case.

Eigenstates of the system of interest are obtained by imaginary-time propagation of a proper Hamiltonian with a Gaussian wave packet as an initial state. Singularities in Coulomb-type potential terms are removed by replacing $1/x \to 1/\sqrt{x^2+\epsilon^2}$ (softening of the potential is applied in both real- and imaginary-time evolution). A soft-core parameter ϵ^2 is chosen to align the ground-state energy with the value of the full quantum problem at hand, in our case the ground state of He. That ensures the ionization potential of the different models compared to be similar. Small changes of ϵ^2 in quantum calculations only qualitatively affect the results obtained. In classical simulations the soft-core parameter plays the same role as in quantum simulations, but in this case, in

order to "stabilize" the atom and prevent the autoionization process from taking place, it must belong to a certain range of values that are usually higher than for the quantum models.

In the following we consider a linearly polarized laser pulse, described by an electric-field component of the form

$$F(t) = F_0 f(t) \sin(\omega t + \phi), \tag{3}$$

where F_0, $f(t)$, ω, and ϕ are the field amplitude, the time-dependent envelope, the frequency, and the carrier-envelope phase of the pulse, respectively. For comparison of different models we take a laser pulse with the frequency $\omega = 0.06$ (corresponding roughly to the wavelength of 800 nm), the phase $\phi = 0$, and the sine-squared envelope

$$f(t) = \sin^2\left(\frac{\pi t}{T}\right), \tag{4}$$

where $T = 2\pi n/\omega$ is the duration of an n-cycle pulse. Here we take $n = 4$ as a typical value. To prevent a nonphysical reflection of the wave function from boundaries of the numerical grid, absorbing boundary conditions are applied, i.e., starting from a fixed distance from the edge of integration region, the wave function is multiplied by a function that smoothly decreases in the direction of boundaries.

B. Algorithm for the Eckhardt-Sacha model

The Eckhardt-Sacha model [24] assumes that the ionization of atoms occurs mainly along two directions $\mathbf{r}_1$ and $\mathbf{r}_2$, forming an angle $\pi/6$ with the z axis, due to the location of saddle points of the energy surface. The resulting 2D Hamiltonian, in the length gauge, may be written as

$$H = \sum_{i=1}^{2}\left(\frac{p_i^2}{2} - \frac{2}{\sqrt{r_i^2+\epsilon^2}} + \frac{F(t)\sqrt{3}}{2} r_i\right) + \frac{1}{\sqrt{(r_1-r_2)^2 + r_1 r_2 + \epsilon^2}}, \tag{5}$$

where $F(t)$ is the electric field value, r_i and p_i are the position and momentum operators for both electrons, and ϵ^2 is the parameter introduced to soften the Coulomb singularity in the reduced-dimensionality model.

In order to obtain the wave-function evolution in time one splits the Hamiltonian into kinetic and potential parts and uses Eq. (1). It is worth noting that the evolution of the kinetic part is efficiently done in momentum space, as it reduces to a simple multiplication, whereas the evolution of the potential part is best computed in a coordinate representation [11]. This strategy allows one to eliminate the numerical differentiation and thus to increase the precision of calculations. The transformation between these representations is realized via fast Fourier transform routines.

Ionization yields are calculated by integrating probability fluxes through borders between different spatial areas corresponding to a stable atom (A) or a single- (S_i) and a double- (D_i) ionization event, as depicted in Fig. 1. The method, originally proposed by Dundas *et al.* [40], was extended in [11,12] in a way that allowed one to distinguish between direct and indirect double-ionization events. That is accomplished due to different values of parameters a and b, defining different

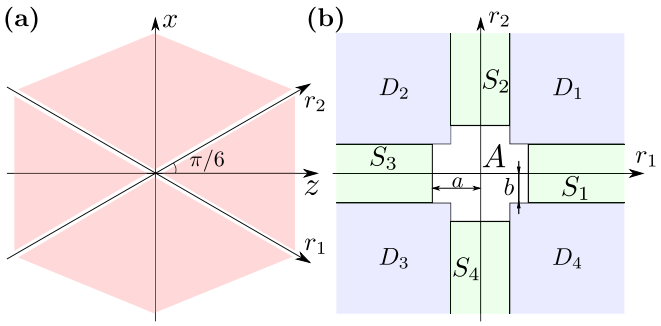

FIG. 1. Geometry of the ES model. (a) Saddle tracks forming the directions along which electrons are allowed to move. The polarization axis points along z. (b) Different regions of the configuration space used to define the state of the system: the neutral atom A, singly charged ions S_i, and doubly charged ions D_i. The parameters are $a = 12.5$ a.u. and $b = 6$ a.u.

regions in the configuration space. In particular, for $b < a$ simultaneous double-ionization events can be detected as transitions across the common border between a neutral atom A and regions D_i that correspond to double ionization. For $b = a$ those borders shrink to a point and disappear for $b > a$, requiring more complex indicators for the direct double ionization.

Of course, the choice of a and b affects the results, but fortunately only weakly so. For instance, making them twice as big will change quantitative values for, e.g., ionization yields, but does not, as verified by us, change the qualitative picture and will therefore still allow us to compare the reduced-dimensionality models. The actual values used in our simulations are the same as those taken in previous studies [11,40] for double-ionization studies.

Within the same model it is also possible to obtain momentum distributions, however, a different computational approach is needed [9,12]. First, one needs to rewrite the Hamiltonian (5) in the velocity gauge, where the vector potential is given by

$$A(t) = -\int_0^t F(\tau) d\tau. \tag{6}$$

Next it is assumed that electrons that travel a large distance from the nucleus, say, 200 a.u. and more, experience a negligible Coulomb interaction with the nucleus, are unlikely to turn back, and follow an evolution governed predominantly by the laser field. For such electrons it is then plausible to assume that all Coulomb terms may be ignored, leaving only the kinetic part in the Hamiltonian (recall that now the velocity gauge is used). In such a case, the evolution is efficiently performed in the momentum representation as it reduces to a multiplication by a proper phase factor. Furthermore, evolving the wave function in the momentum representation allows one to keep all information about an infinite position space; no parts of the wave function are lost due to the absorbing boundary conditions. The ES model describes a two-electron system, thus it is necessary to consider also an intermediate case, i.e., when only one electron is far away and the other is still relatively close to the nucleus. In such a case, only the interaction of the distant electron with the nucleus and the other electron is neglected, while the electron close to the

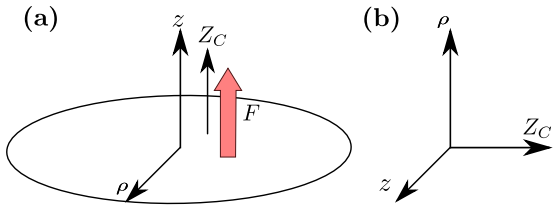

FIG. 2. (a) Geometry of the c.m. model. Here Z_c and z, the directions of the center of mass and the relative electronic coordinate, respectively, are collinear with the electric-field polarization direction; ρ is the cylindrical radial direction of relative motion in the x-y plane. (b) Dimensions for evaluating the problem.

core evolves with the Coulomb electron-nucleus interaction included. Eventually, the full evolution is performed in three different regions, i.e., in a region with both electrons close to the nucleus (evolution with the full Hamiltonian), in a region with one electron close to the nucleus and the other at a larger distance (semiapproximate Hamiltonian), and in a region with two distant electrons (full-approximate Hamiltonian). At the end of the calculations, one collects all parts of the wave functions from the three regions in the momentum representation, while the part related to bound states is smoothly extracted. The squared modulus of the wave function in the momentum space gives a momentum distribution. A detailed description of the method, including the procedure for transferring the wave function between different regions, is presented in [12].

For standard simulations within the ES model the following parameters are used: a soft-core parameter of $\epsilon^2 = 0.6$ (yielding the correct ground-state energy for He), the spatial grid step $\Delta r_1 = \Delta r_2 = 0.2$, and the temporal step of $\Delta t = 0.05$. The computations for an aligned electrons model employ the same algorithm in this work. The change of the system geometry is expressed in the change of the Hamiltonian (5),

$$H = \sum_{i=1}^{2}\left(\frac{p_i^2}{2} - \frac{2}{\sqrt{r_i^2+\epsilon^2}} + F(t)r_i\right) + \frac{1}{\sqrt{(r_1-r_2)^2+\epsilon^2}}. \tag{7}$$

C. Algorithm for the center-of-mass model

The c.m. model follows from the simple observation made by Ruiz *et al.* [26] that classically, in linearly polarized fields, the component of the atomic c.m. momentum perpendicular to the field polarization direction is conserved and thus may be set to zero. For two-electron systems, one of the coordinates then vanishes. The conservation of the angular momentum projection on the polarization z axis reduces the problem further so that only three dimensions out of the initial six remain. They are the relative cylindrical radial coordinate $\rho = |\rho_1 - \rho_2|$ and the field-parallel coordinates z_1 and z_2 of both electrons or, equivalently, $Z_c = (z_1 + z_2)/2$ and $z = (z_1 - z_2)$ for the coordinates of the c.m. and the relative position. The last coordinate pair is useful as the z coordinate decouples from the electric field (see Fig. 2). The momentum operators in the c.m. representation have the forms $\mathbf{P} = \mathbf{p}_1 + \mathbf{p}_2$ and $\mathbf{p} = (\mathbf{p}_1 - \mathbf{p}_2)/2$. The Hamiltonian of the system is then

$$H = H_{Z_c} + H_z + H_\rho, \tag{8}$$

where

$$H_{Z_c} = -\frac{1}{4}\frac{\partial^2}{\partial Z_c^2} + A_Z^2 - iA_Z\frac{\partial}{\partial Z_c} + \frac{1}{3}V,$$
$$H_z = -\frac{\partial^2}{\partial z^2} + \frac{1}{3}V, H_\rho = -\frac{1}{\rho}\frac{\partial}{\partial\rho}\left(\rho\frac{\partial}{\partial\rho}\right) + \frac{1}{3}V, \tag{9}$$

with A_Z the vector potential of the laser field (here the velocity gauge is used, although the length gauge may be used as well) and V the sum of Coulombic interactions

$$V = \frac{1}{\sqrt{z^2+\rho^2}} - \frac{2}{\sqrt{\left(Z_c - \frac{z}{2}\right)^2 + \frac{\rho^2}{4} + \epsilon^2}} - \frac{2}{\sqrt{\left(Z_c + \frac{z}{2}\right)^2 + \frac{\rho^2}{4} + \epsilon^2}}. \tag{10}$$

The TDSE is solved via the operator splitting technique as described above [see Eqs. (1) and (2) for the Hamiltonian (8)]. Note the unusual symmetric distribution of the potential onto all parts in Eq. (9). Elementary unitary steps in Eqs. (1) and (2) are evaluated with the Crank-Nicolson method. It is particularly efficient for this problem as in each unitary step only derivatives along a single coordinate are present, resulting in tridiagonal matrices that may be efficiently inverted. The wave function is defined, of course, on a three-dimensional grid. More details on the algorithm may be found elsewhere [41].

Ionization yields are computed by integrating the wave function in the region $r > 12.5$ a.u.; for calculating the double-ionization yield, the additional conditions used are $\sqrt{z_1^2+\rho^2/4}>z_0$ and $\sqrt{z_2^2+\rho^2/4}>z_0$ as well as $z_0 = 12.5$ a.u. Again, as for the ES model, the choice of z_0 is to some extent arbitrary, so we set $z_0 = a$ (the original proposition of the model [26] uses $z_0 = 12$ a.u.).

For calculating the final momentum distribution, the transformation of the wave function corresponding to the double-ionized state from the coordinate representation to the momentum representation is realized by a fast Fourier transform along the z and Z_c directions and by a Hankel transform along the ρ direction. Such a wave function is obtained by extracting bound states from the full wave function. In our algorithm the spatial criterion for separating bound and free states is used. The part of the wave function corresponding to the region with radius less than the given value z_0 is multiplied by a function that tends to zero in the neighborhood of zero radius and becomes equal to unity when the radius equals z_0. We use a Gaussian function for this purpose, with standard deviation equal to 10 a.u. The value of z_0 for calculating momenta distribution is taken to be 30 a.u. Both the ionization yields and the momentum distributions obtained using our implementation are in agreement with those obtained by the authors of the original algorithm [42]. For standard simulations the following parameters are used: a soft-core parameter of $\epsilon^2 = 0.135$, a spatial grid step $\Delta z = \Delta Z_c = \Delta\rho = 0.3$ a.u., and a temporal step $\Delta t = 0.05$ a.u.

D. Algorithms for classical simulations

Important advantages of classical algorithms in comparison to quantum ones are their higher efficiency and lower requirements for computational resources. They allow one to analyze the original two-electron system without dimensional constraints and for a wide range of field intensities. Due to the classical consideration of electrons motion one can trace back the particular double- or single-ionized trajectory and can deduce additional information about the mechanism of ionization and the preliminary conditions of the system that favor an ionization event.

The classical algorithm for our two-electron system is based on the analysis of the Hamiltonian for the respective model by numerical integration of the canonical equations of motion. As the system which we consider is nonintegrable, special attention should be paid to stability of the numerical algorithm used for its solution [43,44]. In our work the numerical integration was based on the symplectic Runge-Kutta-Nyström algorithm [45] with its parameters chosen properly to give a minimal effective error.

In the most general setting, the studied two-electron system is described by a 6D Hamiltonian of the form

$$H = \sum_{i=1}^{2}\left(\frac{\mathbf{p}_i^2}{2} - \frac{2}{\sqrt{\mathbf{r}_i^2+\epsilon^2}} + \mathbf{F}(t)\cdot\mathbf{r}_i\right) + \frac{1}{\sqrt{(\mathbf{r}_1-\mathbf{r}_2)^2+\epsilon^2}}, \tag{11}$$

where $\mathbf{p}_i = \{p_{x_i}, p_{y_i}, p_{z_i}\}$ and $\mathbf{r}_i = \{x_i, y_i, z_i\}$ are 3D momenta and position vectors of electrons $i = 1$ and 2, respectively.

The initial phase-space coordinates required for integration of the canonical equations of motion are generated by the pilot atom's two-electron trajectory technique at zero-field amplitude [13,14]. The pilot trajectory is started at zero-position-space coordinates, whereas its initial momenta are obtained by random distribution of residual energy E_r, which is the difference between the ground-state energy and a fictitious potential energy arising from including the smoothing factor ϵ, i.e., $E_r = E_g - 1/\epsilon$. The pilot atom's two-electron trajectory is integrated until the energetically allowed position and momentum spaces are fully populated.

To reach the entire population of the energetically allowed space for our case, the pilot atom's trajectory was run for time $t = 10^4$ a.u., producing an ensemble of about 10^7 initial points. The initial coordinates for the pilot atom's two-electron trajectory are chosen randomly. One should note that some alternative techniques for generating initial conditions are possible. An important example is a widely used microcanonical ensemble technique [27,29,31,46]. We implemented and tested both methods and found that the choice between them is irrelevant for generating initial distribution for our problem as both lead to a very similar value of ionization yields. We use the pilot atom's two-electron trajectory technique as it provides much faster calculations. The ground-state energy is set to $E_g = -2.936$ a.u. for all our classical simulations.

In order to obtain reasonable information about ionization yield a large ensemble of 10^7 trajectories is used for calculations in the presence of a laser field. At the end of the pulse, single- and double-ionization events are extracted by applying the spatial criterion; the electron is considered to be ionized if its distance from the nucleus is large, i.e., $r > 100$ a.u.

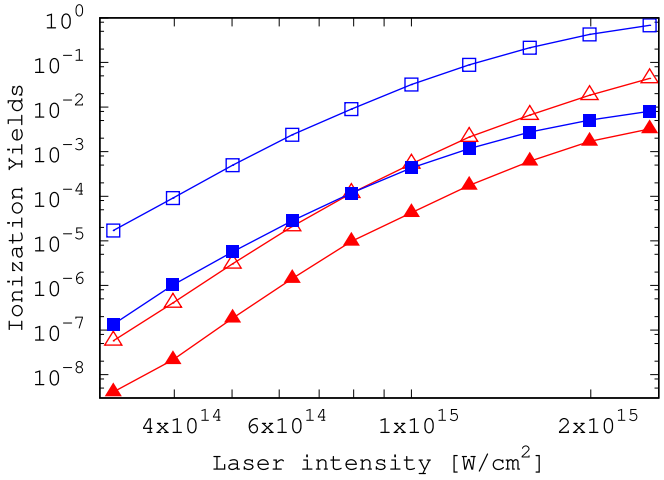

FIG. 3. Single- and double-ionization yields (probability of a given process) as a function of laser field intensity obtained by quantum-mechanical simulations. Single- and double-ionization yields are marked by open and closed symbols, respectively; results for the ES model are marked by blue squares and for the c.m. model by red triangles. In both cases a four-cycle $\sin^2$ pulse was assumed.

In contrast to atoms described in quantum formalism, classical atoms may experience autoionization in the absence of an external field due to intensive many-body Coulombic interactions [47,48]. Such an autoionization may be several orders more intensive than the expected ionization by the external laser field, thus one has to eliminate the effect. It is done by introducing the ϵ term to the Hamiltonian in the same manner as in the quantum-mechanical models. For all our classical simulation we set $\epsilon^2 = 0.6$. Following the method described above, the numerical simulations for the quantum ES, aligned-electron, and c.m. models given by Eqs. (5), (7), and (8), respectively, are reproduced classically in the framework of Hamiltonian dynamics.

III. IONIZATION YIELD COMPARISON

The ionization yield is one of the most important quantities characterizing the ionization dynamics of atomic and molecular systems. In Figs. 3 and 4 one can see the dependence of the ionization yield on the laser field intensity obtained from quantum and classical simulations.

The first striking observation coming from the analysis of both graphs is the low probability of ionization in the c.m. model: For both classical and quantum calculations the yield appears to be less than that for 1D + 1D and for (classical only) 3D + 3D models. This is quite understandable from the classical mechanics. So, let us first explain the difference between c.m. and aligned-electron models, based on geometrical arguments.

The condition of setting the c.m. radial coordinate to zero is in fact a kind of a holonomic constraint. It implies the rule that both electron radial coordinates are the same, up to a sign: $\rho_1 = -\rho_2$. For single ionization the electron's escape is most probable along the z polarization axis, or $\rho_1 \sim \rho_2 \sim 0$. While

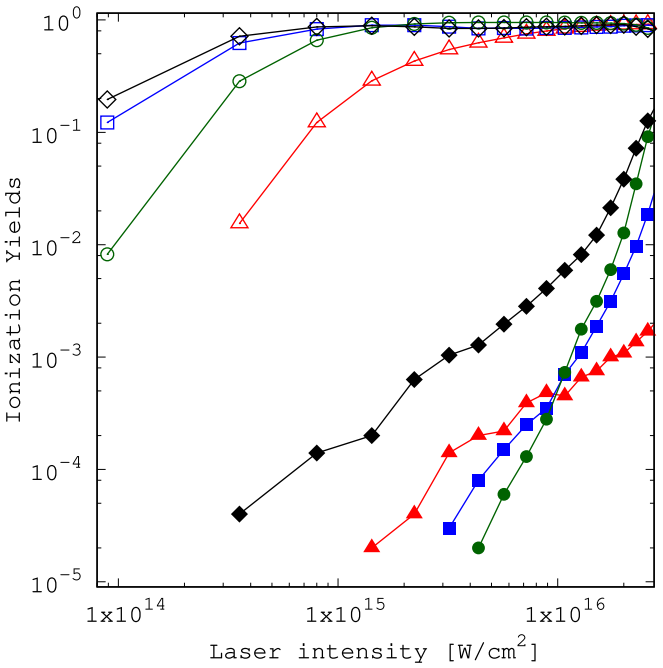

FIG. 4. Single- and double-ionization yields as a function of the laser field intensity obtained by classical simulations. Single- and double-ionization yields are marked by open and closed symbols, respectively; results for the ES model are marked by blue squares, for the c.m. model by red triangles, for the Rochester model by black diamonds, and for the full 3D classical model by green circles. For all the simulations 800-nm four-cycle pulses of $\sin^2$ shape were used.

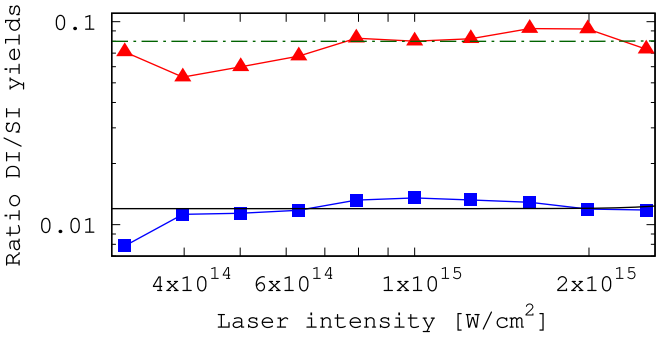

FIG. 5. Ratio of double- to single-ionization yields as a function of the laser field intensity for the c.m. (triangles) and the ES (squares) models obtained by quantum simulations. The solid and dash-dotted lines denote the ratio calculated with the rate equations with constants $C = 0.012$ and $C = 0.08$, respectively.

for the full 6D case this condition by no means restricts the second electron position, in the c.m. case the second electron should have the same radial coordinate. In other words, the number of possible electronic spatial configurations that lead to an escape of an electron is considerably smaller for the c.m. model, resulting in a smaller ionization output.

The same arguments help us understand the c.m. vs 1D + 1D comparison. While for the c.m. case the configurations with $\rho_1 \sim \rho_2 \sim 0$ constitute a minority, for the aligned-electron case the configurations with $\rho_1 = \rho_2 = 0$ are the only possible ones yielding a much larger output. Although the ES 1D + 1D model puts both axes in a nonzero angle to the z axis, in fact it affects only the effective field strength value, multiplying it by a cosine of this angle, thus allowing one to use the same explanation.

The sequential double-ionization yields follow the same scenario: The second electron ionization implies that both electrons are in the neighborhood of the z axis, thus reducing the number of possible configurations and consequently the total yield. At the same time the NSDI signal requires the electron correlation which occurs only when both electrons are close to each other ($\rho_1 - \rho_2 \sim 0$), but once $\rho_1 = -\rho_2$, it leads to the pronounced condition $\rho_1 \sim \rho_2 \sim 0$ and thus a lowered ionization yield. Since all the above explanations are essentially geometrical, they can be applied to the quantum case as well: The quantum data show a similar trend.

The important parameter to look at is the ratio between yields for doubly and singly ionized atoms. Its dependence on field intensity is depicted in Fig. 5. The ratio between double- and single-ionization yields for both algorithms has approximately the same "flat" shape in the regime of intensities studied. It correlates very well with the saturation of that ratio observed in experiments [7] as well as in the double-ionization model [49] based on the rescattering mechanism [50]. On the other hand, such a ratio allows for a quantitative comparison with experiment since volume averaging effects (due to laser intensity variation across the sample), while affecting strongly the yields themselves, may modify this ratio by a factor of 2 at most. Both the experiment [7] and theory [49,51,52] give the saturation value of He^{2+}/He^{+} being of the order of 10^{-3}, an order of magnitude smaller than the ratio obtained for the ES model and almost two orders smaller than this ratio in the c.m. model (compare Fig. 5). This discrepancy again indicates that the predictions of restricted-dimensionality models may be qualitative at best. One could make an attempt to calculate this ratio classically, but Fig. 4 reveals that classical ensemble calculations fail to reproduce any plateau in the ionization yield ratio for the chosen Coulomb smoothing parameter $\epsilon^2 = 0.6$. By allowing for more freedom and using different smoothing parameters for electron-nucleus and electron-electron interactions, one may significantly modify the ratio between doubly and singly ionized species, bringing it closer to experimental values. We mention such a possibility only as we do not want to complicate the studied model further.

It is not surprising that ionization yields deduced from classical simulations are much bigger than those from quantum calculations. This seems to be a general property of all the classical simulations as seen from the comparison of data from classical [34,35,48,53–55] and quantum [9–12,56,57] simulations.

One should note that both quantum algorithms (ES and c.m.) have their limitations on the laser field intensities for which the calculations can be performed. Both algorithms become inadequate at obtaining ionization yields for an electric-field amplitude less than 10^{14} W/cm^2 as any possible reduction of spatial and temporal grid size gives rise to parasitic numerical effects. The c.m. algorithm also has its upper limit on intensity: Larger intensities and laser field wavelengths require larger spatial grid sizes and thus a larger amount of computer memory, as well as computation time. For 800 nm and an intensity of

2.5×10^{15} W/cm^2 in the laser field the converged calculations require already 128 GB of memory.

The Ammosov-Delone-Krainov formula [37] was developed for calculating the rate of single-electron ionization within the single-active-electron approach under the influence of the electric field $F(t)$ [58],

$$W_{ij}^{\mathrm{ADK}} = \left(\frac{3e}{\pi}\right)^{3/2} \frac{j^2}{3n_{ij}^{*3}} \frac{1}{2n_{ij}^{*}-1} \left(\frac{4ej^3}{(2n_{ij}^{*}-1)n_{ij}^{*3}|F|}\right)^{2n_{ij}^{*}-3/2} \times \exp\left(-\frac{2j^3}{3n_{ij}^{*3}|F|}\right), \tag{12}$$

where $j \to i = j-1$ denotes ionization of atoms or ions of charge j and $n_{ij}^{*} = j/\sqrt{2E_{ij}}$ is an effective principal quantum number related to ionization energy $E_{ij} = E_0^{j+} - E_0^{(j-1)+}$. Such a rate can be used for setting the ionization rate equations [59] for populations of the neutral atom P_0, single P_1 ionized ion, or double P_2 ionized ion:

$$\begin{aligned} \dot{P}_0 &= -W_{01}P_0 - W_{02}P_0, \\ \dot{P}_1 &= W_{01}P_0 - W_{12}P_1, \\ \dot{P}_2 &= W_{02}P_0 + W_{12}P_1. \end{aligned} \tag{13}$$

The rate W_{02} of NSDI cannot be determined from the ADK approach, but to determine it we employ the fact that for the region of field amplitudes of interest the sequential double ionization is much less intensive than NSDI and the ratio of He^+ and He^{2+} yields is almost constant. Thus one can set $W_{02} = W_{01}C$, where the constant $C = 0.012$ is defined phenomenologically from TDSE-based ES numerical calculations (see Fig. 5). The results of the straightforward integration of Eqs. (13) is shown in Fig. 6. The resulting curves are sensitive to value of C. To show that we performed the integration of Eqs. (13) with an "incorrect" value of $C = 0.08$ corresponding to data obtained by the c.m. algorithm, the resulting double-ionization curve does not properly fit numerical data.

Surprisingly, the ionization yields obtained with the ADK formula coincide with the ones obtained using the ES algorithm very well. At the same time, the ADK formula is known to fit the full 6D He calculation provided by Parker *et al.* [57]. Thus one can conclude that the ES algorithm provides data that may be qualitatively correct, which is quite a surprising and refreshing result. On the other hand, some of the agreement may be purely accidental.

IV. PHOTOELECTRON MOMENTUM DISTRIBUTION COMPARISON

A study of the momentum distribution is necessary to understand the mechanism of double ionization [19]. It constitutes a cornerstone of the photoelectron holography technique [60]. The ES, aligned-electron, and c.m. methods are able to provide parallel momentum distributions, i.e., a snapshot of electronic wave functions in the momentum representation as a function of the first and second electrons' momenta parallel to the z electric-field direction. The corresponding sample plots are given in Figs. 7(a) and 7(b).

The differences between these two figures can be explained by two factors: technical and geometrical. The first concerns

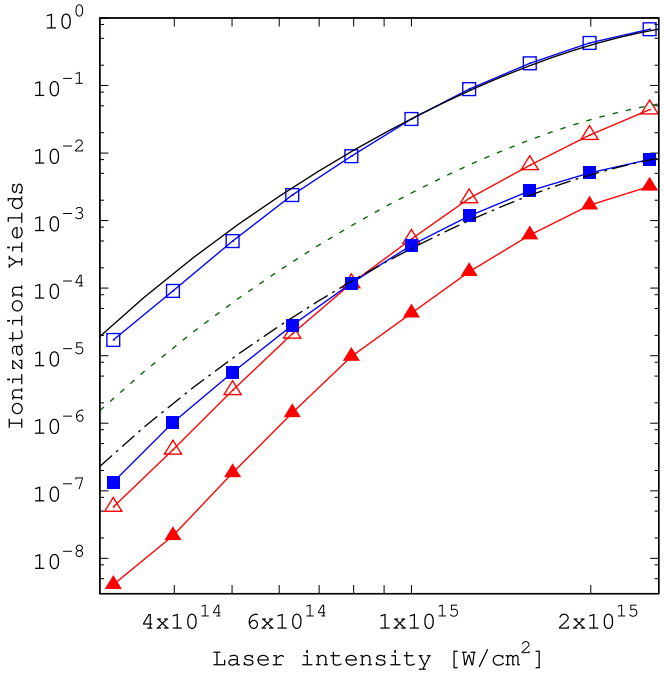

FIG. 6. Single- and double-ionization yields as a function of the laser field intensity. The points correspond to quantum-mechanical simulations as described in Fig. 3. The lines without symbols correspond to yields obtained via the Ammosov-Delone-Krainov formula. The solid line denotes the single-ionization yield. Dash-dotted and dashed lines both correspond to double-ionization yields obtained with correct, $C = 0.012$, and incorrect, $C = 0.08$, coefficients, respectively.

the computation of the wave function in the momentum representation. For the part of the wave function that reached the borders of physical space, the ES algorithm preserves it in the momentum representation. Thus, the information about electrons that escape the computational space before the end of the evolution, and thus presumably the fastest ones, is not lost [12]. Our realization of the c.m. algorithm does not possess such an ability and the information about some portion of fast moving electrons may be missing provided the spatial grid for computations is not large enough.

The geometrical factor explains the presence and intensity of the interference picture. In the ES model the propagation of electronic waves is restricted to the plane, making their interference clear (the corresponding image is not shown) [12,61]. For experimental relevance one should introduce smoothing by Gaussian functions; this is done in Figs. 7(a) and 7(b). Increasing the number of dimensions provides the electronic system with a much larger number of possible quantum paths leading to blurring of the interference structure. In this sense the c.m. model simulations yield more realistic predictions as experiments deal with full 3D problems. The c.m. model is supposed to behave better than the ES one when multidimensional details of electron-core rescattering processes are needed, e.g., for problems of photoelectron holography.

One should note that as the c.m. code is evaluated in the coordinate representation, for the sake of accounting for all the produced photoelectron momenta, one should keep the coordinate space rather large to not let any part of the wave function

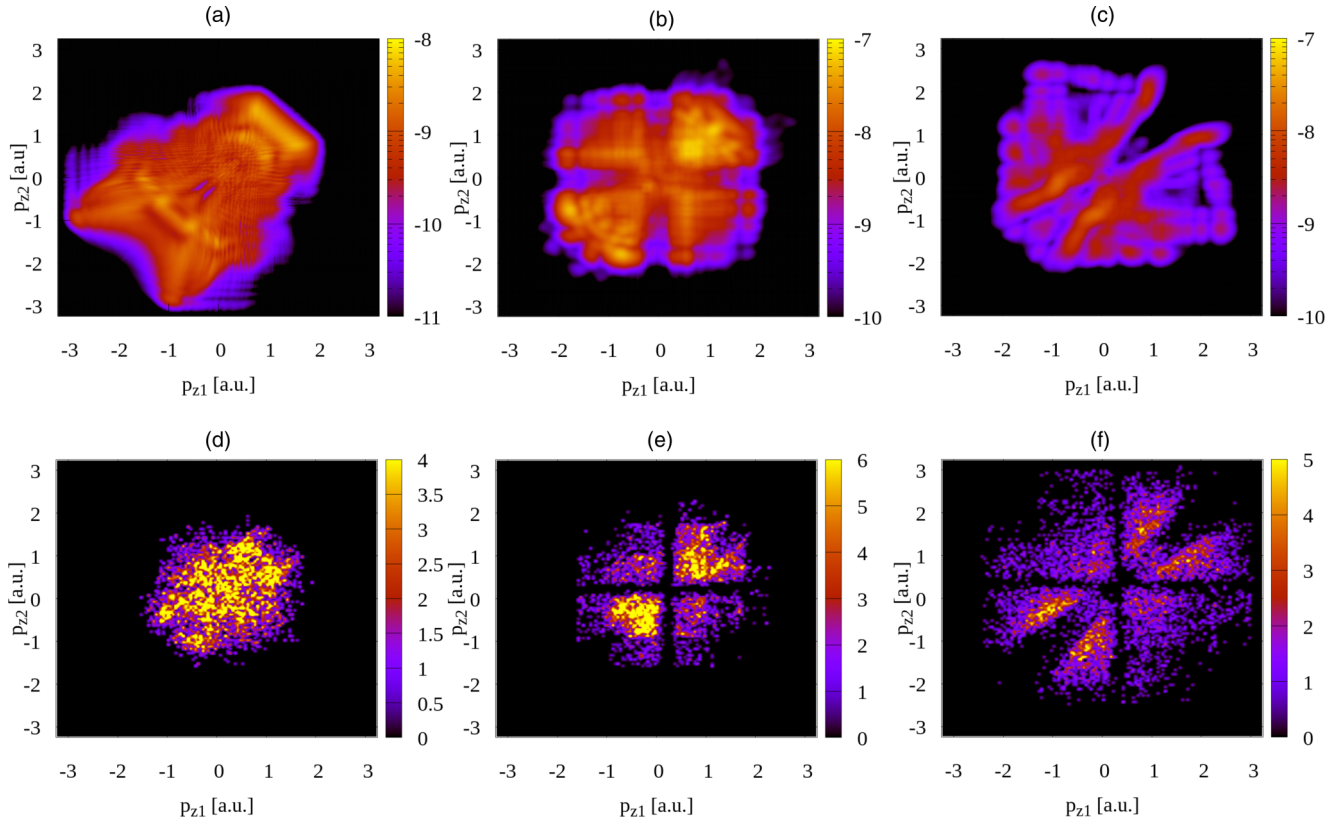

FIG. 7. Released electron momentum distribution computed with (a)–(c) quantum and (d)–(f) classical simulations for (a) and (d) the c.m., (b) and (e) the ES, and (c) and (f) the aligned electron models. Simulations were done for the 800-nm field of intensity 6.3×10^{14} W/cm^2. The parameters of the grid for quantum models are, for the ES and the aligned electron plot, 4096×4096 points with coordinate step size 100/512 a.u., and for the c.m. model, $3372 \times 1686 \times 454$ points with coordinate step size 0.3 a.u.; the laser pulse consists of four cycles. The plots in (b) and (c) are smoothed with Gaussian functions 0.12 a.u. wide. The value of $\epsilon^2 = 0.58$ in (c) corresponds to the same energy of the ground state as in (b). Classical data were obtained with the use of (d) 4×10^7 sample trajectories for the c.m. model, (e) 4×10^7 sample trajectories for the ES model, and (f) 5×10^6 sample trajectories for the aligned electron model. For classical simulations the same spatial criterion of the double-ionization event was used and an eight-cycle laser pulse was applied.

escape from it. Thus, with the same set of parameters given, calculating momentum distributions requires many times larger spatial grids than calculating ionization yields or high-harmonic spectra. The ES algorithm does not have such a complication, as the part of the electronic wave function that moved far enough from the atomic core is then treated in the momentum representation, which requires a relatively small grid size.

On the other hand, the ES algorithm suffers from the problem of the "empty cross" in the momentum distribution plot [12]. The cross occupies space along the p_{r_1} and p_{r_2} axes; the wave function inside it has a magnitude many orders smaller than in the neighboring regions. It arises from cutting the wave function, in the coordinate representation, in the area with coordinates close to zero. It is this area that contains most of the low-momentum electrons. Thus one should be careful extracting the bounded part of the wave function. We have found that for the ES model the optimal value of distance at which the cutting is performed is 50 a.u. The c.m. algorithm is affected by this feature much less, mostly because electrons with zero momentum p_z are not restricted to be in the close neighborhood of the atomic core, but can stay far from it due to the ρ coordinate.

The described factor is also geometrical and can be illustrated with classical trajectory calculations. In Figs. 7(d) and 7(e) one can see two plots for the z-axis momentum distribution of two electrons for the same problem studied. First, one can note that the general shape of the distribution is quite similar to that of the quantum case in Figs. 7(a) and 7(b). This leads to the conclusion that the classical calculations are much more appropriate in studies of electronic momentum distributions than for ionization yield studies. Second, the cross in the momentum distribution is present quite prominently in both the ES and aligned electron cases and it arises for the same reason: Electrons with $p_r \sim 0$ are located in the area $r \sim 0$. For this set of classical calculations the length of the laser pulse was taken to be twice as large as that for the quantum computations, as it is hard to collect enough double-ionization events for a four-cycle pulse.

One may observe, furthermore, that quantum momentum distributions for the same intensity are significantly larger than classical ones. This is a phenomenon often observed in classical-quantum comparisons (see, e.g., [62]) and may be attributed to quantum tunneling that allows one to explore the momentum space forbidden by classical mechanics.

In addition, an obvious signature of very strong electronic repulsion in the aligned electron model can be found by analyzing momentum distributions. In Figs. 7(c) and 7(f) one can see the pronounced low-probability area along the $p_{z1} = p_{z2}$ direction. Releasing electrons with the same momenta would mean having their positions close to each other, which is quite unlikely due to the electron repulsion.

V. CONCLUSION

As mentioned in the Introduction, a study of two-electron ionization in strong laser fields at infrared frequencies is beyond the reach of full quantum simulations. There are several possible reduced-dimensionality models with different features and different numbers of dimensions. We have compared in our work three of the most popular choices for such models. The aligned-electron model (the Rochester model) gives unrealistic electron momentum distributions because the Coulomb repulsion suppresses the experimentally observed dominance of equal-momentum events. Here the Eckhardt-Sacha model provides a significant improvement, with the same number of degrees of freedom and the same numerical complexity. Moreover, it performs remarkably well in comparison with the ADK model for the calculation of electron ionization yields.

The center-of-mass model has one degree of freedom more (three instead of two) and necessarily it is more demanding in terms of the computer time and memory. The ionization yields given by both the Eckhardt-Sacha and center-of-mass models give qualitative trends of similar accuracy. Single-electron yields are also in qualitative agreement with the ADK theory. For momentum distribution the center-of-mass model yields results in closer agreement with experiments; for the Eckhardt-Sacha model additional smoothing simulating experimental resolution is needed to remove a pronounced interference pattern.

Most of the differences between those two models can be understood with the application of geometric reasoning. In this sense, the classical trajectory simulations of multiple-electron ionization provided evidence for the above explanations. The calculations have also shown that classical trajectory simulations can reproduce the distributions of electron momenta in strong fields.

In our analysis of the models, we have focused on the two most important observables: the ionization yield and the final electron momentum distribution. The case of higher-harmonic generation requires further study.

ACKNOWLEDGMENTS

We are grateful to Joe Eberly for comments at the early stages of this work and to Jesse Mumford for his help with preparing the manuscript. Support from PL-Grid Infrastructure is acknowledged. This work was realized under National Science Centre (Poland) Project Symfonia No. 2016/20/W/ST4/00314 (D.K.E., J.S.P.-B., M.L., and J.Z.) and No. 2015/19/B/ST2/01028 (A.M.). M.L. acknowledges also MINECO (National Plan 15 Grant FISICATEAMO No. FIS2016-79508-P, Grants No. SEVERO OCHOA No. SEV-2015-0522, FPI), European Social Fund, Fundació Cellex, Generalitat de Catalunya (AGAUR Grant No. 2017 SGR1341 and CERCA/Program), ERC AdG OSYRIS, and EU FETPRO QUIC. A.C. thanks Los Alamos National Laboratory, which is operated by LANS, LLC, for the NNSA of the U.S. DOE under Contract No. DE-AC52-06NA25396.

[1] J. S. Parker, E. S. Smyth, and K. T. Taylor, J. Phys. B **31**, L571 (1998).
[2] J. S. Parker, D. Glass, L. R. Moore, E. S. Smyth, K. Taylor, and P. Burke, J. Phys. B **33**, L239 (2000).
[3] K. C. Kulander, K. J. Schafer, and J. L. Krause, *Atoms in Intense Laser Fields* (Academic, New York, 1992).
[4] J. Feist, S. Nagele, R. Pazourek, E. Persson, B. I. Schneider, L. A. Collins, and J. Burgdörfer, Phys. Rev. A **77**, 043420 (2008).
[5] J. M. N. Djiokap, A. V. Meremianin, N. L. Manakov, S. X. Hu, L. B. Madsen, and A. F. Starace, Phys. Rev. A **96**, 013405 (2017).
[6] W. Becker, X. Liu, P. J. Ho, and J. H. Eberly, Rev. Mod. Phys. **84**, 1011 (2012).
[7] B. Walker, B. Sheehy, L. F. DiMauro, P. Agostini, K. J. Schafer, and K. C. Kulander, Phys. Rev. Lett. **73**, 1227 (1994).
[8] D. N. Fittinghoff, P. R. Bolton, B. Chang, and K. C. Kulander, Phys. Rev. Lett. **69**, 2642 (1992).
[9] M. Lein, E. K. U. Gross, and V. Engel, Phys. Rev. Lett. **85**, 4707 (2000).
[10] C. Ruiz, L. Plaja, J. R. Vázquez de Aldana, and L. Roso, Phys. Rev. A **68**, 023409 (2003).
[11] J. S. Prauzner-Bechcicki, K. Sacha, B. Eckhardt, and J. Zakrzewski, Phys. Rev. Lett. **98**, 203002 (2007).
[12] J. S. Prauzner-Bechcicki, K. Sacha, B. Eckhardt, and J. Zakrzewski, Phys. Rev. A **78**, 013419 (2008).
[13] R. Panfili, J. H. Eberly, and S. L. Haan, Opt. Express **8**, 431 (2001).
[14] R. Panfili, S. L. Haan, and J. H. Eberly, Phys. Rev. Lett. **89**, 113001 (2002).
[15] T. Weber, H. Giessen, M. Weckenbrock, G. Urbasch, A. Staudte, L. Spielberger, O. Jagutzki, V. Mergel, M. Vollmer, and R. Dörner, Nature (London) **405**, 658 (2000).
[16] A. Rudenko, V. L. B. de Jesus, T. Ergler, K. Zrost, B. Feuerstein, C. D. Schröter, R. Moshammer, and J. Ullrich, Phys. Rev. Lett. **99**, 263003 (2007).
[17] M. Kübel, K. Betsch, N. G. Kling, A. Alnaser, J. Schmidt, U. Kleineberg, Y. Deng, I. Ben-Itzhak, G. Paulus, T. Pfeifer *et al.*, New J. Phys. **16**, 033008 (2014).
[18] N. Camus, B. Fischer, M. Kremer, V. Sharma, A. Rudenko, B. Bergues, M. Kübel, N. G. Johnson, M. F. Kling, T. Pfeifer *et al.*, Phys. Rev. Lett. **108**, 073003 (2012).
[19] A. Staudte, C. Ruiz, M. Schöffler, S. Schössler, D. Zeidler, T. Weber, M. Meckel, D. Villeneuve, P. Corkum, A. Becker *et al.*, Phys. Rev. Lett. **99**, 263002 (2007).
[20] D. F. Ye, X. Liu, and J. Liu, Phys. Rev. Lett. **101**, 233003 (2008).

[21] P. Koval, F. Wilken, D. Bauer, and C. H. Keitel, Phys. Rev. Lett. **98**, 043904 (2007).
[22] D. Bauer, Phys. Rev. A **56**, 3028 (1997).
[23] Y. Chen, Y. Zhou, Y. Li, M. Li, P. Lan, and P. Lu, Phys. Rev. A **97**, 013428 (2018).
[24] K. Sacha and B. Eckhardt, Phys. Rev. A **63**, 043414 (2001).
[25] B. Eckhardt, J. S. Prauzner-Bechcicki, K. Sacha, and J. Zakrzewski, Chem. Phys. **370**, 168 (2010).
[26] C. Ruiz, L. Plaja, L. Roso, and A. Becker, Phys. Rev. Lett. **96**, 053001 (2006).
[27] J. Leopold and I. C. Percival, J. Phys. B **12**, 709 (1979).
[28] J. Grochmalicki, M. Lewenstein, and K. Rzążewski, Phys. Rev. Lett. **66**, 1038 (1991).
[29] M. Gajda, J. Grochmalicki, M. Lewenstein, and K. Rzążewski, Phys. Rev. A **46**, 1638 (1992).
[30] K. Rzążewski, M. Lewenstein, and P. Salières, Phys. Rev. A **49**, 1196 (1994).
[31] M. Wójcik, J. Zakrzewski, and K. Rzążewski, Phys. Rev. A **52**, R2523 (1995).
[32] P. J. Ho and J. Eberly, Opt. Express **15**, 1845 (2007).
[33] J. Chen, J. Liu, L. B. Fu, and W. M. Zheng, Phys. Rev. A **63**, 011404 (2000).
[34] P. J. Ho, R. Panfili, S. L. Haan, and J. H. Eberly, Phys. Rev. Lett. **94**, 093002 (2005).
[35] F. Mauger, C. Chandre, and T. Uzer, Phys. Rev. Lett. **102**, 173002 (2009).
[36] S. A. Berman, J. Dubois, C. Chandre, M. Perin, and T. Uzer, Phys. Rev. A **97**, 061402(R) (2018).
[37] M. Ammosov, N. Delone, and Krainov, Sov. Phys. JETP **64**, 1191 (1986).
[38] K. Kondo, A. Sagisaka, T. Tamida, Y. Nabekawa, and S. Watanabe, Phys. Rev. A **48**, R2531 (1993).
[39] S. Larochelle, A. Talebpour, and S.-L. Chin, J. Phys. B **31**, 1201 (1998).
[40] D. Dundas, K. T. Taylor, J. S. Parker, and E. S. Smyth, J. Phys. B **32**, L231 (1999).
[41] A. Chacón Salazar, Interaction of attosecond and femtosecond pulses with atoms and molecules, Ph.D. thesis, Universidad de Salamanca, 2014.
[42] S. Chen, C. Ruiz, and A. Becker, Phys. Rev. A **82**, 033426 (2010).
[43] E. Hairer, C. Lubich, and G. Wanner, *Geometric Numerical Integration: Structure-Preserving Algorithms for Ordinary Differential Equations*, Springer Series in Computational Mathematics Vol. 31 (Springer, Berlin, 2006).
[44] D. Efimov, N. Bezuglov, A. Klyucharev, Y. N. Gnedin, K. Miculis, and A. Ekers, Opt. Spectrosc. **117**, 8 (2014).
[45] S. Blanes and P. Moan, J. Comput. Appl. Math. **142**, 313 (2002).
[46] F. Mauger, C. Chandre, and T. Uzer, J. Phys. B **42**, 165602 (2009).
[47] S. L. Haan, R. Grobe, and J. H. Eberly, Phys. Rev. A **50**, 378 (1994).
[48] F. Mauger, C. Chandre, and T. Uzer, Phys. Rev. Lett. **105**, 083002 (2010).
[49] V. R. Bhardwaj, S. A. Aseyev, M. Mehendale, G. L. Yudin, D. M. Villeneuve, D. M. Rayner, M. Y. Ivanov, and P. B. Corkum, Phys. Rev. Lett. **86**, 3522 (2001).
[50] P. B. Corkum, Phys. Rev. Lett. **71**, 1994 (1993).
[51] G. L. Yudin and M. Y. Ivanov, Phys. Rev. A **63**, 033404 (2001).
[52] Z. Chen, X. Li, O. Zatsarinny, K. Bartschat, and C. D. Lin, Phys. Rev. A **97**, 013425 (2018).
[53] P. J. Ho and J. H. Eberly, Phys. Rev. Lett. **95**, 193002 (2005).
[54] P. J. Ho and J. H. Eberly, Phys. Rev. Lett. **97**, 083001 (2006).
[55] F. Mauger, C. Chandre, and T. Uzer, Phys. Rev. Lett. **104**, 043005 (2010).
[56] M. Brics, J. Rapp, and D. Bauer, Phys. Rev. A **90**, 053418 (2014).
[57] J. S. Parker, K. J. Meharg, G. A. McKenna, and K. T. Taylor, J. Phys. B **40**, 1729 (2007).
[58] F. Ilkov, J. Decker, and S. Chin, J. Phys. B **25**, 4005 (1992).
[59] A. l'Huillier, L. A. Lompre, G. Mainfray, and C. Manus, Phys. Rev. A **27**, 2503 (1983).
[60] Y. Huismans, A. Rouzée, A. Gijsbertsen, J. Jungmann, A. Smolkowska, P. Logman, F. Lepine, C. Cauchy, S. Zamith, T. Marchenko *et al.*, Science **331**, 61 (2011).
[61] T. Shaaran, C. Figueira de Morisson Faria, and H. Schomerus, Phys. Rev. A **85**, 023423 (2012).
[62] V. Ayadi, P. Földi, P. Dombi, and K. Tőkési, J. Phys. B **50**, 085005 (2017).